



Properties of $\text{Bi}_{0.8}\text{Ln}_{0.2}\text{FeO}_3$ ($\text{Ln}=\text{La, Gd, Ho}$) multiferroic ceramics

Fei Xue^b, Qiuyun Fu^{a,b,*}, Dongxiang Zhou^{a,b}, Yahui Tian^b, Yunxiang Hu^b, Zhiping Zheng^b, Ling Zhou^b

^aState Key Laboratory of Material Processing and Die & Mould Technology, Huazhong University of Science and Technology, Wuhan 430074, PR China

^bSchool of Optical and Electronic Information, Huazhong University of Science and Technology, Wuhan 430074, PR China

Received 30 May 2015; received in revised form 29 July 2015; accepted 30 July 2015

Available online 8 August 2015

Abstract

$\text{Bi}_{0.8}\text{Ln}_{0.2}\text{FeO}_3$ ($\text{Ln}=\text{La, Gd, Ho}$) multiferroic ceramics were prepared by a solid state reaction method and their properties were investigated in detail. In the Rietveld refinements of the XRD data for these ceramics, good agreement between the measured and calculated patterns was observed. The leakage current density and resistivity of ceramics were analyzed, and it was found that $\text{Bi}_{0.8}\text{Ho}_{0.2}\text{FeO}_3$ (BHFO) ceramics possessed much better electric insulation than $\text{Bi}_{0.8}\text{La}_{0.2}\text{FeO}_3$ (BLFO) and $\text{Bi}_{0.8}\text{Gd}_{0.2}\text{FeO}_3$ (BGFO) ceramics. Considerable differences in magnetic properties among BLFO, BGFO, and BHFO ceramics were observed and might be correlated with the suppression of the spatially modulated spiral spin structure. A notable exchange bias effect was observed in these ceramics at room temperature, which may be correlated with exchange interaction at the interfaces of weakly ferromagnetic and antiferromagnetic components. Moreover, the magnetoelectric (ME) coupling effect was confirmed in $\text{Bi}_{0.8}\text{Ln}_{0.2}\text{FeO}_3$ ($\text{Ln}=\text{La, Gd, Ho}$) ceramics by the magnetic field induced polarization and dielectric investigations.

© 2015 Elsevier Ltd and Techna Group S.r.l. All rights reserved.

Keywords: Rietveld refinements; Multiferroic; Exchange bias; Magnetoelectric

1. Introduction

Multiferroics have attracted ever-increasing attention in recent years because of the potential applications in novel magnetoelectric (ME) devices, such as multiple-state ME memory, which will exponentially improve computing capacity [1]. The perovskite BiFeO_3 is a promising multiferroic material, having ferroelectric (FE) ordering below the Curie transition temperature $T_C \sim 1103$ K and a G type antiferromagnetic (AFM) transition at $T_N \sim 643$ K [2]. It is ferroelectricity originated from the stereochemically active $6s^2$ lone pair of Bi^{3+} , and the G-type AFM is derived from the partially filled 3d orbitals of the Fe^{3+} ions [3,4]. Since its discovery in the 1960s, three crucial problems have hampered its practical applications, including difficulties in: (1) synthesizing single-phase samples due to the volatilization of Bi_2O_3 and its metastable state, (2) observing the ferroelectric loop because of its

low resistivity, and (3) deriving weak ferromagnetism owing to the existence of spiral spin modulation that results in minuscule net magnetization (ca. $10^{-6} \mu_B$ per Fe^{3+} ion) [3,5].

The problem 1 and 2 can be solved using rapid liquid-phase sintering and La^{3+} substitution of Bi^{3+} [2,6]. In addition, lanthanides doping is an effective method to improve the magnetization of BiFeO_3 (problem 3), and mainly two explanations for the origin of spontaneous magnetization are proposed: (1) suppressing the space-modulation spin structure of BiFeO_3 by the crystal lattice distortion [7,8], (2) introducing additional magnetic moment [9,10]. For the selected La^{3+} , Gd^{3+} , and Ho^{3+} elements, the ionic radii in 8-fold coordination and effect magnetic moments are 1.16 Å (0 μ_B), 1.053 Å (7.94 μ_B), and 1.015 Å (10.6 μ_B), respectively, and we expect to determine which is the main reason of the abovementioned two for the net magnetization in lanthanides doping.

Moreover, characterization of magnetoelectric (ME) coupling requires measuring the effect of a magnetic field on ferroelectric polarization or, conversely, that of an electric field

*Tel.: +86 27 87558482, +86 18602717211; fax: +86 27 87558482.

E-mail address: fugy@mail.hust.edu.cn (Q. Fu).

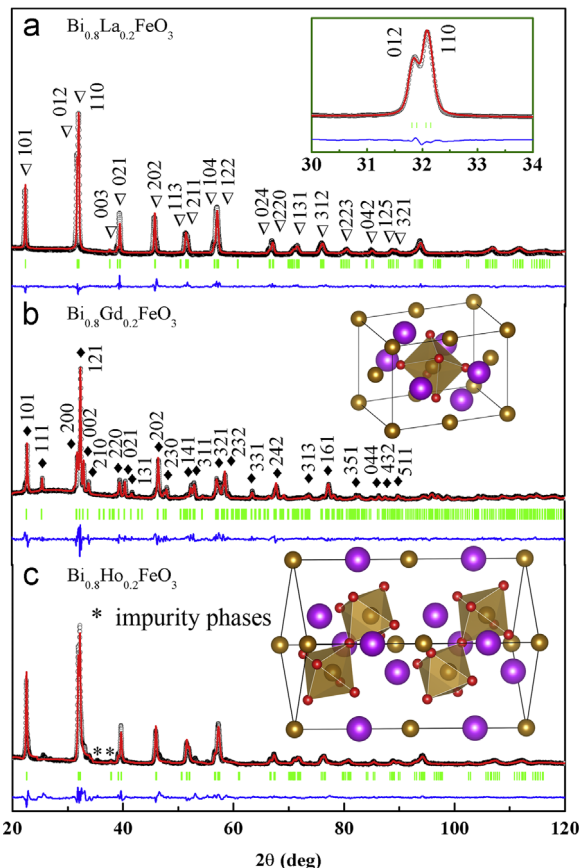


Fig. 1. Observed (hollow circles), calculated (solid line), and their difference (solid line at the bottom) XRD patterns for $\text{Bi}_{0.8}\text{Ln}_{0.2}\text{FeO}_3$ ceramics. Bragg reflections are indicated by sticks.

on magnetic order [7,11,12]. Since magnetic field can induce the variation in polarization, the field can also indirectly alter the dielectric constant of ME multiferroics, which is called magentodielectric (MD) effect. Thus, a widely used alternative characterization method consists in measuring the dielectric constant (ϵ') under magnetic field [13]. In this work, we report the preparation of La^{3+} ($4f^0$), Gd^{3+} ($4f^7$), and Ho^{3+} ($4f^{10}$) doped BiFeO_3 ceramics via the solid state method and conventional sintering process, and systematically investigated their phase composition, ferroelectromagnetic behaviors, and MD properties.

2. Experimental

Ceramic samples of $\text{Bi}_{0.8}\text{La}_{0.2}\text{FeO}_3$ (BLFO), $\text{Bi}_{0.8}\text{Gd}_{0.2}\text{FeO}_3$ (BGFO), and $\text{Bi}_{0.8}\text{Ho}_{0.2}\text{FeO}_3$ (BHFO) were prepared by conventional sintering process using high-purity Bi_2O_3 , La_2O_3 , Gd_2O_3 , Ho_2O_3 , and Fe_2O_3 reagents as starting materials. The raw materials were ball milled with alcohol, dried, and calcined. The calcined mixtures were then ball milled again, dry pressed, and sintered. To synthesize single-phase samples, the sintering temperatures were carefully selected; the highest sintering temperature was 855°C . Finally, the samples were polished with silver paste to form two electrodes.

The crystal structure of the samples was characterized by an X-ray diffractometer (XRD, Empyrean) using $\text{Cu K}\alpha$ radiation ($\lambda=1.54505\text{ \AA}$). Simulation of crystal structure based on the measured XRD patterns was carried out using a Rietveld crystal structure refinement software named as General Structure Analysis System (GSAS). The morphology and grain size were examined using a field emission scanning electron microscope (FESEM, Nova NonoSEM 450). The magentodielectric (MD) effect of these samples was determined by a low-frequency impedance analyzer (WK-6500B), with an applied voltage of 1 V and applied magnetic field of 3 kOe. The leakage current density and ferroelectric hysteresis loops were recorded using a ferroelectric measuring system (Multiferroic, Radiant Technologies, Inc.). The magnetic hysteresis loop was measured by a vibrating sample magnetometer (VSM, LakeShore 7400). All these measurements were carried out at room temperature.

3. Results and discussion

Fig. 1 shows the results of the Rietveld refinements of the XRD data for the BLFO, BGFO, and BHFO ceramic samples. From the figure, BLFO and BHFO ceramics show a rhombohedral structure with space group $R\bar{3}c$ (JCPDS 15-4394), while BGFO ceramics show an orthorhombic phase with space group

Table 1
Refined structural parameters of BLFO, BGFO, and BHFO samples.

Structure parameters	Bi _{0.8} La _{0.2} FeO ₃ <i>R</i> 3c	Bi _{0.8} Gd _{0.2} FeO ₃ <i>Pnma</i>	Bi _{0.8} Ho _{0.2} FeO ₃ <i>R</i> 3c
Lattice parameters (Å)			
<i>a</i> (Å)	5.5771 (4)	5.6238 (6)	5.5626(6)
<i>b</i> (Å)	5.5771 (4)	7.8064 (8)	5.5626(6)
<i>c</i> (Å)	13.8205 (10)	5.4274 (6)	13.8123 (12)
<i>V</i> (Å ³)	372.27	238.27	370.12
<i>c/a</i>	2.395	0.965	2.483
<i>R</i> -factors (%)			
<i>R</i> _p	3.16	3.26	3.79
<i>R</i> _{wp}	4.57	4.85	5.64
χ^2	2.56	2.68	2.76
Atomic position parameters			
Bi/La/Ho/Gd			
<i>x</i>	0	0.4528	0
<i>y</i>	0	0.25	0
<i>z</i>	0.22023	0.0067	0.22017
Fe			
<i>x</i>	0	0	0
<i>y</i>	0	0	0
<i>z</i>	0	0	0
O			
<i>x</i>	O ₁	O ₂	
<i>y</i>	0.0929	0.1988	0.5305
<i>z</i>	0.3126	0.0344	0.25
	0.10211	0.295	0.6068
0.0938			0.3158
0.1021			
Interatomic distances (Å)			
Bi–O	2.252	2.430	2.262
Fe–O	1.961	1.971	1.943
	2.097	2.044	2.104
Fe–O–Fe angle (°)	154.663	153.396	154.835

Pnma (JCPDS 16-6040). Small additional peaks are associated with the trace of mullite-type Bi₂Fe₄O₉ (JCPDS 20-0836) and sillenite-type Bi₂₅FeO₃₉ (JCPDS 78-1543) impurity phases, which were also reported in Ref. [9].

The crystal structure parameters derived from the refinements are summarized in Table 1. Fittings of XRD profiles for BLFO and BHFO ceramics were performed using the rhombohedral system (*R*3c) in a hexagonal setting, while for BGFO ceramics using the orthorhombic system (*Pnma*). As can be seen, the calculated XRD patterns coincide well with the measured XRD patterns with small *R* values (*R*_{wp} ≤ 5.64%, *R*_p ≤ 3.79%). Generally, to calculate the values of *c_{pc}*/*a_{pc}*, the rhombohedral cell parameters are expressed in the pseudocubic cell: *a_{pc}*=*a_{hex}*/√2 and *c_{pc}*=*c_{hex}*/(2√3) [14,15], and the ratio *c_{pc}*/*a_{pc}* increases from 1.0115 for bulk BLFO to 1.0136 for BHFO.

The variations in the refined structural parameters are related with Goldschmidt tolerance factor *t*. The tolerance factor *t* of ABO₃ perovskites can be written as:

$$t = \frac{r_A + r_O}{\sqrt{2}(r_B + r_O)}; \quad (1)$$

where *r_A*, *r_B*, and *r_O* are the respective ionic radii. In BLFO, because of the same ionic radius (1.36 Å) of La³⁺ and Bi³⁺ in

12-fold coordination [16,17], its tolerance factor (*t*=0.954) is comparable to the reported one of BiFeO₃ (*t*=0.96) ceramics [18], and its polar *R*3c structure is stabilized primarily due to stereochemical activity of the lone pairs of the Bi³⁺ ions [9]. While, substitutions of the smaller Ho³⁺ and Gd³⁺ ions for bigger Bi³⁺ ions on the A-sites are expected to suppress the Bi–O hybridization reducing the activity of the lone-pair and consequently canceling the long-range ferroelectric ordering in the compounds. Indeed, the calculated values of the Bi–O bond lengths in Table 1 shows upward trend on Ho³⁺ and Gd³⁺ doping comparing to La³⁺ doping.

Cross-sectional FESEM images of the BLFO, BGFO, and BHFO ceramics are shown in Fig. 2. It is clear from the FESEM images that BLFO ceramics possess the largest grains with an average diameter of ~3.5 μm. It can also be seen that, apart from closely piled grains, a certain amount of intergranular pores are seen in BGFO ceramics. Density measurements using the Archimedes' method show that the BLFO ceramics have the highest density ($\rho=8.05 \times 10^3 \text{ kg/m}^3$). The apparent densities of the BGFO and BHFO ceramics are $7.58 \times 10^3 \text{ kg/m}^3$ and $7.85 \times 10^3 \text{ kg/m}^3$, respectively.

Fig. 3(a) shows the leakage current density *J* of the BLFO, BGFO, and BHFO ceramics as a function of the electric field *E*, whereas the dependences of the resistivity *R* of the BLFO, BGFO,

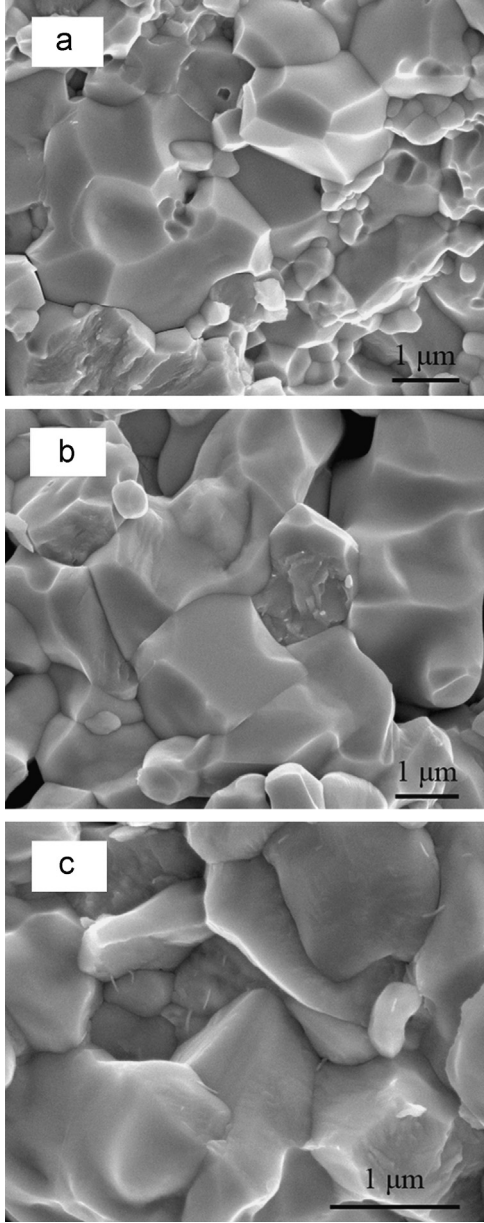


Fig. 2. Cross-sectional FESEM images of (a) BLFO, (b) BGFO, and (c) BHFO ceramics.

and BHFO ceramics on the electric field E are shown in Fig. 3(b). Obviously, except for the BHFO ceramics, all the ceramics exhibit the high J values of 1.513×10^{-4} – $7.504 \times 10^{-5} \text{ A/cm}^2$ and low R values of 1.535×10^8 – $3.076 \times 10^8 \Omega \text{ cm}$ under the electric field of 40 kV/cm , indicating that BHFO ceramics possess much better electric insulation than BLFO and BGFO ceramics.

Fig. 4(a) shows the M – H hysteresis for all the specimens at room temperature, and the magnetization data are summarized in Table 2. As can be seen, BHFO ceramics have the largest remnant magnetization of 87.6 memu/g and saturation magnetization of 1.61 emu/g , showing a weak ferromagnetism. The enhanced magnetization in BHFO is not caused by the $\text{Bi}_2\text{Fe}_4\text{O}_9$ and $\text{Bi}_{25}\text{FeO}_{39}$ impurities, because, $\text{Bi}_{25}\text{FeO}_{39}$ is a paramagnetic at 5 – 950 K , and $\text{Bi}_2\text{Fe}_4\text{O}_9$ is an antiferromagnet

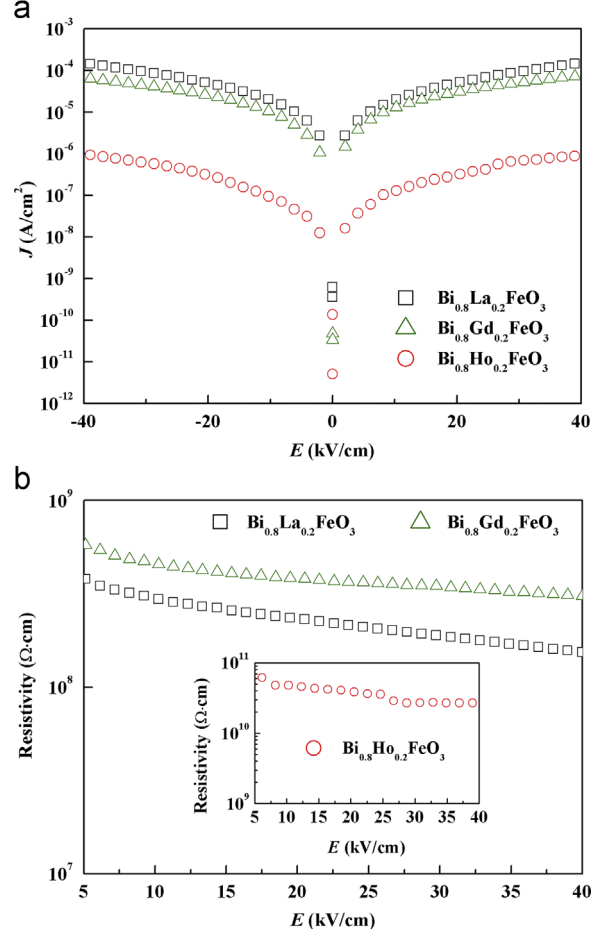


Fig. 3. (a) Leakage current density J and (b) resistivity R of $\text{Bi}_{0.8}\text{Ln}_{0.2}\text{FeO}_3$ ceramics as a function of the electric field E .

with a Néel temperature of 258 K [19,20], both of them show a poor magnetic properties.

The origin of the spontaneous magnetization in BiFeO_3 system is mainly explained as the suppression of spin structure [7,11,21]. Whereas, the mechanism of the spontaneous magnetization in lanthanides doped BiFeO_3 is more complex. Zhou et al. [10] have reported that the exchange interaction between Er 4f electrons and Fe 3d electrons may also partly contributed to the enhanced magnetization, on the other hand, Khomchenko et al. have pointed out that Gd^{3+} magnetic moments cannot contribute to nonzero remanent magnetization and significant coercivity in $\text{Bi}_{0.8}\text{Gd}_{0.2}\text{FeO}_3$ if the spiral spin modulation in iron sublattice remains unsuppressed [22]. Thus, the origination of the spontaneous magnetization for lanthanides doping needs further theoretical investigation. In BLFO and BGFO ceramics, the number of 4f electrons for La^{3+} and Gd^{3+} ions is quite different ($4f^0$ and $4f^7$), but these two samples show a similar magnetic behaviors. Besides, Gd^{3+} and Ho^{3+} ions have a similar the number of 4f electrons ($4f^7$ and $4f^{10}$), but BGFO and BHFO ceramics show quite different magnetic properties. From the results of the Rietveld refinements, we can also find that BHFO ceramics with strong magnetism possess high value of $c_{\text{pc}}/a_{\text{pc}}$ (1.0136), which

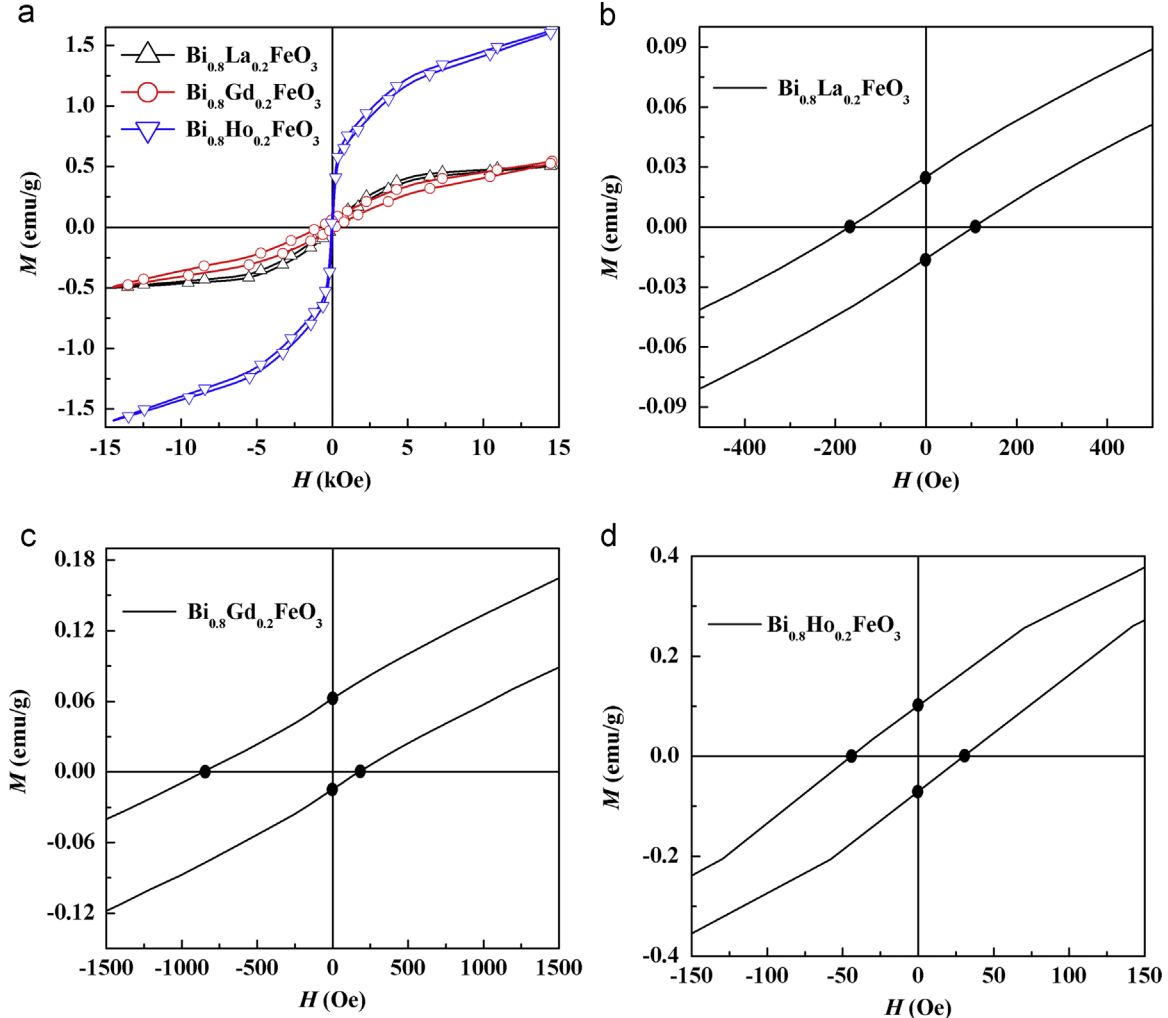


Fig. 4. (a) M - H hysteresis curve, and (b)–(d) enlarged view of H_{EB} for $\text{Bi}_{0.8}\text{Ln}_{0.2}\text{FeO}_3$ ceramics.

Table 2

The remnant magnetization M_r , saturation magnetization M_s , exchange bias H_{EB} and vertical shift M_{shift} of BLFO, BGFO, and BHFO ceramics.

	M_r (memu/g)	M_s (emu/g)	H_{EB} (Oe)	H_{EB}/H_C (%)	M_{shift} (memu/g)
BLFO	20.5	0.506	30	21.46	3.88
BGFO	38.6	0.521	330	64.15	23.7
BHFO	87.6	1.612	7	18.67	15.88

means a large crystal distortion, thus a big Fe–O–Fe angle (154.84°) was induced. Therefore, the considerable differences in magnetic properties among BLFO, BGFO, and BHFO ceramics are mainly associated with the structure-distortion-induced suppression of spiral spin modulation rather than the exchange interaction between 4f electrons and Fe 3d electrons.

The EB field H_{EB} is generally defined as $H_{\text{EB}}=(H_{c1}+H_{c2})/2$, where H_{c1} and H_{c2} are the left and right coercive fields [23], respectively, as shown by solid circles in Fig. 4(b)–(d). The vertical shift is defined as $M_{\text{shift}}=(M_{r1}+M_{r2})/2$, where M_{r1} and M_{r2} are the magnetization with positive and negative points of intersection

[24], respectively. Calculated values of H_{EB} and M_{shift} for BLFO, BGFO, and BHFO ceramics are summarized in Table 2. The exchange bias phenomena were also reported in the similar $\text{Bi}_{0.2}\text{La}_{0.8}\text{Fe}_{1-x}\text{Mn}_x\text{O}_3$ and $\text{Bi}_{0.9}\text{Gd}_{0.1}\text{Fe}_{1-x}\text{Ti}_x\text{O}_3$ ceramics [24,25]. It is expected that the presence of EB phenomenon in $\text{Bi}_{0.8}\text{Ln}_{0.2}\text{FeO}_3$ ceramics originates from the exchange interaction at the interfaces of weakly ferromagnetic and antiferromagnetic components.

Fig. 5(a) shows the hysteresis loops of polarization versus electric field (P - E) for BLFO, BGFO, and BHFO ceramics. Because of the high porosity ($\sim 4\%$, 9% , and 6% for BLFO,

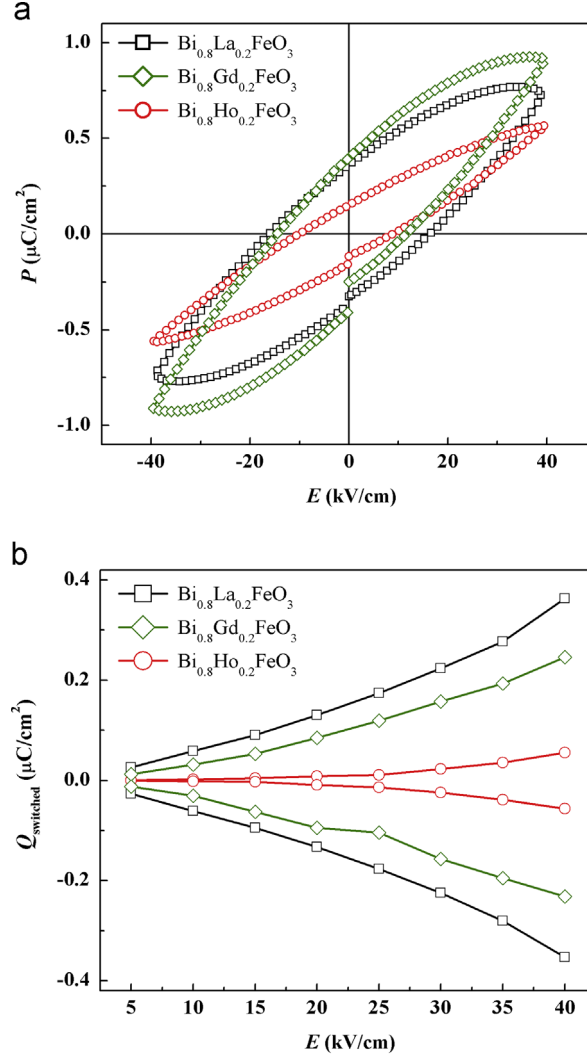


Fig. 5. (a) $P-E$ hysteresis loops and (b) PUND data for $\text{Bi}_{0.8}\text{Ln}_{0.2}\text{FeO}_3$ ceramics.

BGFO, and BHFO, respectively), the hysteresis loops of these ceramics are not saturated and polarization values in sub-coercive region remain very low. More work should be done, for example, using rapid liquid-phase sintering process, or preparing ceramic samples using coprecipitation powder [26], to improve the density.

Whereas, in a measured $P-E$ data, there can be contributions from leakage current, in addition to the switched charge density [2]. To rule out the possibility of artificial polarization from leakage current, we have carried out PUND measurements with the pulse width of 20 ms and pulse delay of 1 ms. Fig. 5(b) shows the PUND data as a function of applied electric field for BLFO, BGFO, and BHFO ceramics. As can be seen, pulsed remnant polarization values Q_{switched} (=switched polarization (P^*) – non-switched polarization (P)) are much smaller for BHFO ceramics, which is attributed to the existence of impurity phases ($\text{Bi}_2\text{Fe}_4\text{O}_9$ and $\text{Bi}_{25}\text{FeO}_{39}$) [26,27]. Meanwhile, the ferroelectricity confirmed by PUND measurements in these ceramics comes from the $6s^2$ lone pairs in Bi^{3+} [4].

To examine the ME coupling effects of BLFO, BGFO, and BHFO ceramics, the changes of electric hysteresis loops (Fig. 6)

and dielectric constant (Fig. 7) as various applied bias magnetic fields were measured. From Fig. 6(a)–(c), we observed an obvious decrease in remnant polarization induced by the bias magnetic field for BHFO ceramics. Fig. 6(d) shows the changes of measured maximum polarization $\Delta P_m (=P_m(3 \text{ kOe}) - P_m(0 \text{ Oe}))$ and changes of remnant polarization $\Delta P_r (=P_r(3 \text{ kOe}) - P_r(0 \text{ Oe}))$ as functions of the electric field E . There is an obvious decrease in remnant polarization P_r from 0.152 to 0.114 $\mu\text{C}/\text{cm}^2$ for BHFO ceramics, and an obvious decrease in P_m from 0.77 to 0.73 $\mu\text{C}/\text{cm}^2$ for BLFO ceramics under the magnetic field [12,28].

Fig. 7(a)–(c) shows the frequency dependence of relative dielectric constant ϵ' under zero and 3 kOe magnetic field. It is clear that the application of the magnetic field induces an increase in ϵ' of the BLFO, BGFO, and BHFO ceramics, respectively. Since the dielectric constant is obviously altered by a magnetic field, it is necessary to calculate the magnetodielectric (MD) effect, defined as [29]

$$\frac{\Delta \epsilon(B)}{\epsilon(0)} = \frac{\epsilon(B) - \epsilon(0)}{\epsilon(0)} \times 100\%, \quad (2)$$

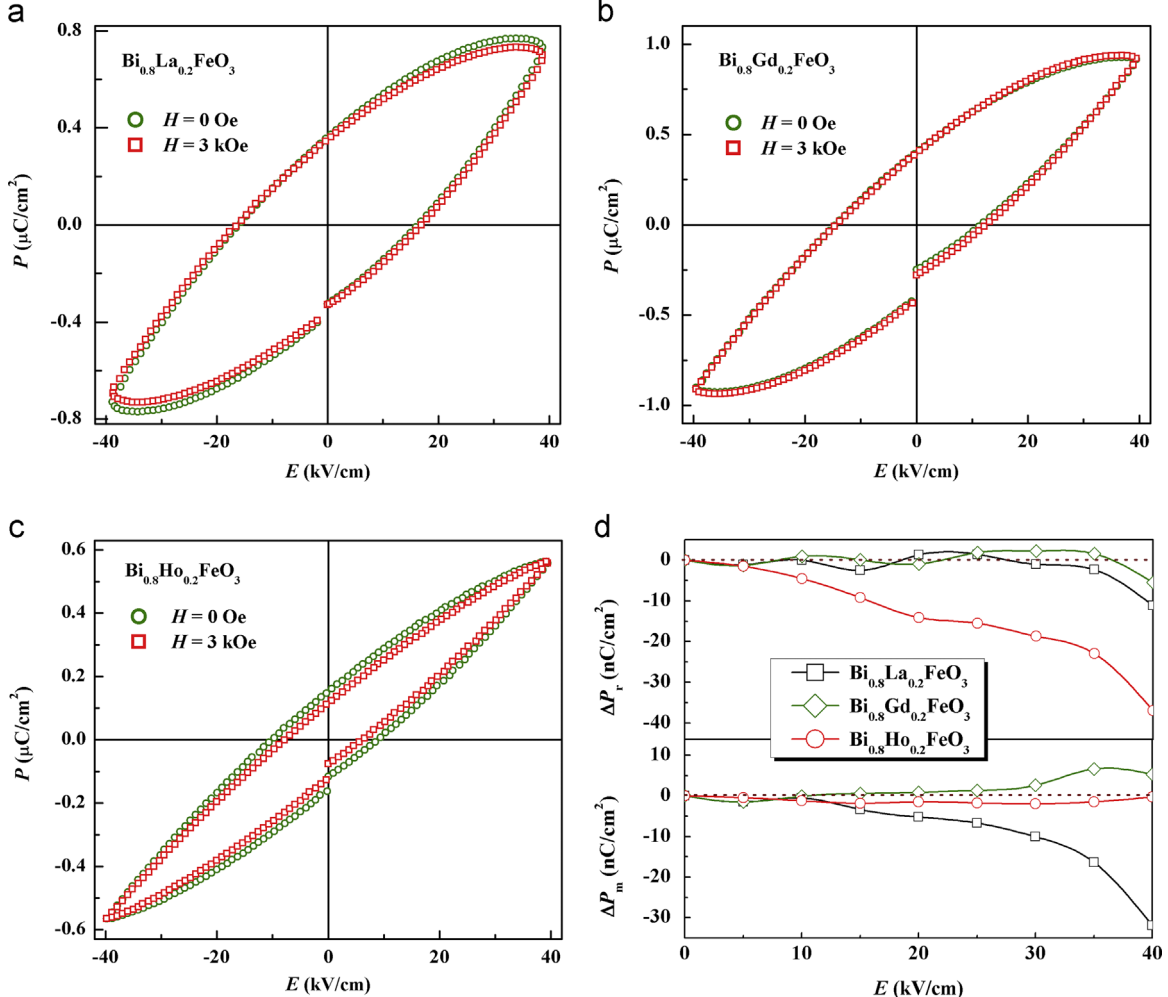


Fig. 6. (a)–(c) P - E hysteresis loops without and with an external magnetic field, (d) ΔP_r and ΔP_m as a function of electric field E .

and the results are shown in Fig. 7(d). For these ceramics, large positive MD values (1–6%) are obtained, which are comparable to the reported ones in the Ni-doped BiFeO_3 ceramics ($B=9 \text{ kOe}$) and Z-type hexaferrite $\text{Sr}_3\text{Co}_2\text{Fe}_{24}\text{O}_{41}$ ($B=5 \text{ T}$) [13,30]. As reported by other researchers [13], the intrinsic MD effect can be explained in terms of the spin-phonon coupling scenario. The phonon frequency can be changed by magnetic fields, which leads to the intrinsic MD effect. While, for the MD effect, three features are noteworthy: (1) magnetoresistance (MR) can yield MD, (2) the sign of the MD depends on whether the MR takes place at the interfaces or at the core, and (3) the MR directly affects the dielectric loss [30,31].

To examine the MR effect, impedance spectroscopy of the samples was conducted with and without magnetic field in the frequency range of 100 kHz–10 MHz, and the results are presented in the form of Cole–Cole plots (Insets of Fig. 7(a)–(c)). It can be seen that the magnetic field has obvious effect on the Cole–Cole plots, displaying a linear reducing tail at lower frequencies, which means an increase in the static resistance when applying a 3 kOe magnetic field. The MD

effect at lower frequency may be contributed to the combination of the Maxwell–Wagner space charge effect and/or magnetoresistance [32].

4. Conclusions

In summary, single-phase BLFO, BGFO, and BHFO multi-ferroic ceramics were successfully prepared by the solid-state reaction method. $\text{Bi}_{0.8}\text{Ln}_{0.2}\text{FeO}_3$ ($\text{Ln}=\text{La}, \text{Gd}, \text{Ho}$) ceramics have realized the coexistence of ferroelectricity and weak ferromagnetism. The enhancement of the magnetization may be correlated with the structure-distortion-induced suppression of spiral spin modulation. The exchange bias effect observed in these ceramics at room temperature may be correlated with exchange interaction at the interfaces of weakly ferromagnetic and antiferromagnetic components. The MD effect at lower frequency may be contributed to the combination of the Maxwell–Wagner space charge effect and/or magnetoresistance.

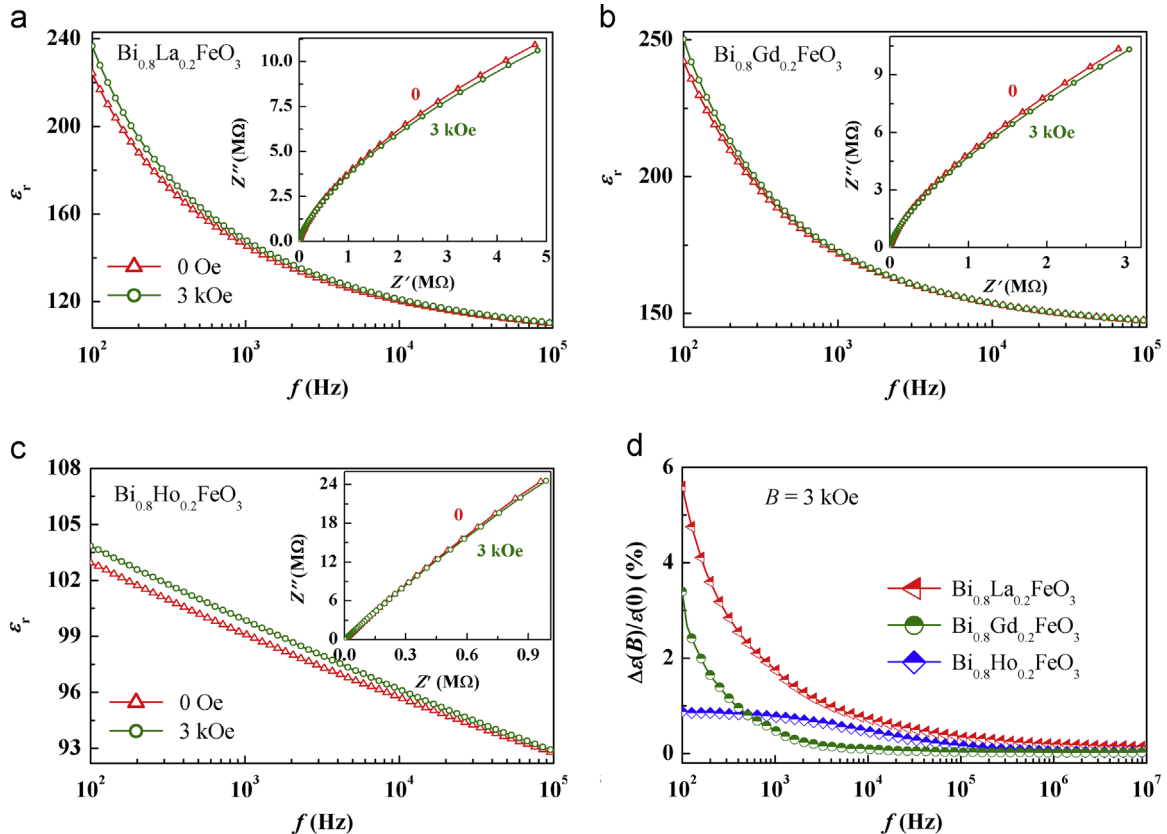


Fig. 7. (a)–(c) and insets show the frequency dependence of ϵ' and impedance $Z'-Z''$ plots under zero and 3 kOe field and (d) frequency dependence of MD effect.

Acknowledgments

This work is financially supported by National Natural Science Foundation of China (Grant no. 61571203) and National High Technology Research and Development Program of China (863 Program No. 2013AA030903). The authors acknowledge the assistance by the Analytical and Testing Center of Huazhong University of Science and Technology.

References

- [1] J.F. Scott, Data storage: multiferroic memories, *Nat. Mater.* 6 (2007) 256.
- [2] Z.W. Lei, Y. Huang, M. Liu, W. Ge, Y.H. Ling, R.R. Peng, X.Y. Mao, X.B. Chen, Y.L. Lu, Ferroelectric and ferromagnetic properties of $\text{Bi}_{7-x}\text{La}_x\text{Fe}_{1.5}\text{Co}_{1.5}\text{Ti}_3\text{O}_{21}$ ceramics prepared by the hot-press method, *J. Alloy. Compd.* 600 (2014) 168.
- [3] K.S. Nalwa, A. Garg, Phase evolution, magnetic and electrical properties in Sm-doped bismuth ferrite, *J. Appl. Phys.* 103 (2008) 044101.
- [4] K.F. Wang, J.M. Liu, Z.F. Ren, Multiferroicity: the coupling between magnetic and polarization order, *Adv. Phys.* 58 (2009) 321.
- [5] G. Catalan, J.F. Scott, Physics and applications of bismuth ferrite, *Adv. Mater.* 21 (2009) 2463.
- [6] S.R. Das, R.N.P. Choudhary, P. Bhattacharya, R.S. Katiyara, P. Dutta, A. Manivannan, M.S. Seehra, Structural and multiferroic properties of La-modified BiFeO_3 ceramics, *J. Appl. Phys.* 101 (2007) 034104.
- [7] F. Xue, Q.Y. Fu, D.X. Zhou, L. Zhou, Y.X. Hu, Z.P. Zheng, G. Jian, L.B. Hao, Structural evolution and physical properties of multiferroic $\text{Bi}_{0.9-x}\text{La}_{0.1}\text{Pb}_x\text{Fe}_{3-x/2}\text{O}_3$ ceramics, *J. Phys. D: Appl. Phys.* 48 (2015) 305004.
- [8] G.L. Yuan, S. Wing, J.M. Liu, Z.G. Liu, Structural transformation and ferroelectromagnetic behavior in single-phase $\text{Bi}_{1-x}\text{Nd}_x\text{FeO}_3$ multiferroic ceramics, *Appl. Phys. Lett.* 89 (2006) 052905.
- [9] V. Kovala, I. Skorvanek, M. Rebec, L. Mitoseriu, H. Yan, Effect of dysprosium substitution on crystal structure and physical properties of multiferroic BiFeO_3 ceramics, *J. Eur. Ceram. Soc.* 34 (2014) 641.
- [10] H.F. Zhou, Z.L. Hou, L.B. Kong, H.B. Jin, M.S. Cao, X. Qi, Enhanced magnetization and improved leakage in Er-doped BiFeO_3 nanoparticles, *Phys. Status Solidi A* 210 (2013) 809.
- [11] Q.Y. Fu, F. Xue, Z.P. Zheng, D.X. Zhou, L. Zhou, Y.H. Tian, Y.X. Hu, Magnetocapacitance and structureproperties of $\text{Bi}_{0.85-x}\text{La}_{0.15}\text{Pb}_x\text{FeO}_3$ ceramics, *Ceram. Int.* 41 (2015) 4050.
- [12] L. Zhou, Q.Y. Fu, D.X. Zhou, F. Xue, Y.H. Tian, L.B. Hao, Magneto-electric coupling study in multiferroic $\text{La}_{0.7}\text{Ba}_{0.3}\text{MnO}_3-\text{BaTiO}_3$ composite ceramic at room temperature, *Ceram. Int.* 41 (2015) 2367–2372.
- [13] X. Zhang, Y.G. Zhao, Y.F. Cui, L.D. Ye, J.W. Wang, S. Zhang, H.Y. Zhang, M.H. Zhu, Magnetodielectric effect in Z-type hexaferrite, *Appl. Phys. Lett.* 100 (2012) 032901.
- [14] K. Chakrabarti, K. Das, B. Sarkar, S. Ghosh, S.K. De, G. Sinha, J. Lahtinen, Enhanced magnetic and dielectric properties of Eu and Co co-doped BiFeO_3 nanoparticles, *Appl. Phys. Lett.* 101 (2012) 042401.
- [15] J. Chaigneau, R. Haumont, J.M. Kiat, Ferroelectric order stability in the $\text{Bi}_{1-x}\text{Pb}_x\text{FeO}_3$ solid solution, *Phys. Rev. B* 80 (2009) 184107.
- [16] D. Kan, L. Pálová, V. Anbusathaiah, C.J. Cheng, S. Fujino, V. Nagarajan, K.M. Rabe, I. Takeuchi, Universal behavior and electric-field-induced structural transition in rare-earth-substituted BiFeO_3 , *Adv. Funct. Mater.* 20 (2010) 1108.
- [17] R.D. Shannon, Revised effective ionic radii and systematic studies of interatomic distances in halides and chalcogenides, *Acta. Cryst. A32* (1976) 751.
- [18] Y. Wan, Y. Li, Q. Li, W. Zhou, Q.J. Zheng, X.C. Wu, C.G. Xu, B.P. Zhu, D.M. Lin, Microstructure, ferroelectric, piezoelectric, and

- ferromagnetic properties of Sc-modified $\text{BiFeO}_3\text{--BaTiO}_3$ multiferroic ceramics with MnO_2 addition, *J. Am. Ceram. Soc.* 97 (2014) 1809.
- [19] A.A. Zatsiupa, L.A. Bashkirov, I.O. Troyanchuk, G.S. Petrov, A.I. Galyas, L.S. Lobanovskii, S.V. Trukhanov, I.M. Sirota, Magnetization, magnetic susceptibility, and effective magnetic moment of the Fe^{3+} ions in $\text{Bi}_2\text{Fe}_4\text{O}_9$, *Inorg. Mater.* 49 (2013) 616.
- [20] A.A. Zatsiupa, L.A. Bashkirov, I.O. Troyanchuk, G.S. Petrov, A.I. Galyas, L.S. Lobanovsky, S.V. Truhanov, Magnetization, magnetic susceptibility, effective magnetic moment of Fe^{3+} ions in $\text{Bi}_{25}\text{FeO}_{39}$ ferrite, *J. Solid. State. Chem.* 212 (2014) 147.
- [21] V.A. Khomchenko, D.A. Kiselev, J.M. Vieira, L. Jian, A.L. Kholkin, A.M.L. Lopes, Y.G. Pogorelov, J.P. Araujo, M. Maglione, Effect of diamagnetic Ca, Sr, Pb, and Ba substitution on the crystal structure and multiferroic properties of the BiFeO_3 perovskite, *J. Appl. Phys.* 103 (2008) 024105.
- [22] V.A. Khomchenko, D.A. Kiselev, I.K. Bdikin, V.V. Shvartsman, P. Borisov, W. Kleemann, J.M. Vieira, A.L. Kholkin, Crystal structure and multiferroic properties of Gd-substituted BiFeO_3 , *Appl. Phys. Lett.* 93 (2008) 262905.
- [23] S.M. Wu, S.A. Cybart, P. Yu, M.D. Rossell, J.X. Zhang, R. Ramesh, R.C. Dynes, Reversible electric control of exchange bias in a multiferroic field-effect device, *Nat. Mater.* 9 (2010) 756.
- [24] M.A. Basith, O. Kurni, M.S. Alam, B.L. Sinha, B. Ahmmad, Room temperature dielectric and magnetic properties of Gd and Ti co-doped BiFeO_3 ceramics, *J. Appl. Phys.* 115 (2014) 024102.
- [25] G. Anjum, R. Kumar, S. Mollah, D.K. Shukla, S. Kumar, C.G. Lee, Structural, dielectric, and magnetic properties of $\text{La}_{0.8}\text{Bi}_{0.2}\text{Fe}_{1-x}\text{Mn}_x\text{O}_3$ ($0 \leq x \leq 0.4$) multiferroics, *J. Appl. Phys.* 107 (2010) 103916.
- [26] J.C. Chen, J.M. Wu, Dielectric properties and ac conductivities of dense single-phased BiFeO_3 ceramics, *Appl. Phys. Lett.* 91 (2007) 182903.
- [27] J. Ryu, C.W. Baek, Y.S. Lee, N.K. Oh, G.F. Han, J.W. Kim, B.D. Hahn, J.J. Choi, W.H. Yoon, J.H. Choi, D.S. Park, D.Y. Jeong, Enhancement of multiferroic properties in $\text{BiFeO}_3\text{--Ba}(\text{Cu}_{1/3}\text{Nb}_{2/3})\text{O}_3$: film fabricated by aerosol deposition, *J. Am. Ceram. Soc.* 94 (2011) 355.
- [28] G. Jian, D.X. Zhou, J.Y. Yang, H. Shao, F. Xue, Q.Y. Fu, Microstructure and multiferroic properties of $\text{BaTiO}_3/\text{CoFe}_2\text{O}_4$ films on $\text{Al}_2\text{O}_3/\text{Pt}$ substrates fabricated by electrophoretic deposition, *J. Eur. Ceram. Soc.* 33 (2013) 1155–1163.
- [29] G. Catalan, Magnetocapacitance without magnetoelectric coupling, *Appl. Phys. Lett.* 88 (2006) 102902.
- [30] A. Kumar, K.L. Yadav, A systematic study on magnetic, dielectric and magnetocapacitance properties of Ni doped bismuth ferrite, *J. Phys. Chem. Solids* 72 (2011) 1189.
- [31] N. Ortega, A. Kumar, R.S. Katiyar, J.F. Scott, Maxwell–Wagner space charge effects on the $\text{Pb}(\text{Zr}, \text{Ti})\text{O}_3\text{--CoFe}_2\text{O}_4$ multilayers, *Appl. Phys. Lett.* 91 (2007) 102902.
- [32] Z.X. Cheng, H. Shen, J.Y. Xu, P. Liu, S.J. Zhang, J.L. Wang, X.L. Wang, S.X. Dou, Magnetocapacitance effect in nonmultiferroic YFeO_3 single crystal, *J. Appl. Phys.* 111 (2012) 034103.